Fractaile Magnetodynamics: Quantized Harmonic Coupling Between Satellite and Ground Magnetospheres

Nowlin 2025 · FUNt October Edition

Abstract

By synchronizing satellite and ground-based magnetometer data, φ-series (Fractaile Ratio) harmonic structure is detected in near-Earth magnetic oscillations. These Harmonic Resonance Bands (HRBs) demonstrate quantized coherence between orbital Hp measurements and ground ΔH, enabling predictive space-weather modeling. A mathematical walk-through of the φ-scaling law shows empirical alignment across multiple datasets, including coupling to magnetotunnelling dynamics.

Definitions

Fractaile — Self-similar, quantized harmonic structure preserving proportional geometry across scales with discrete nodal boundaries; here, the coupled Earth–Sun magnetic lattice.

Fractaile Ratio (φ-Scaling Law) — Fixed geometric proportion ($\varphi \approx 1.618$) governing recursive harmonics in Fractaile systems. Used instead of Golden Ratio to emphasize empirical scaling.

Harmonic Resonance Bands (HRBs) — Quantized frequency bands observed in magnetic-field data, corresponding to discrete φ-series harmonics within the Fractaile lattice.

1 · Introduction

Conventional space-weather models treat geomagnetic variability as stochastic. Joint analysis of GOES Hp and ground ΔH reveals coherent φ-series harmonics indicative of a nested resonant cavity—unified here as Fractaile Magnetodynamics (FMD).

2 · Methods

Data: GOES primary magnetometer Hp and differential electron flux, plus ground ΔH from geomagnetic stations.

Processing: short rolling averages, conservative peak spacing, cross-correlation for lag estimation.

Testing: amplitude steps checked against φ-series multiples (φ^0, φ^1, φ^2,…).

3 · Results (Summary)

We observe

(i) repeatable peak spacing forming φ-series ladders,

(ii) consistent electron lag relative to Hp (buffered response),

(iii) amplitude clustering near φ^k bands.

Findings persist across quiet and disturbed intervals—consistent with a resonant-cavity interpretation.

Figure 1 — FUNt Harmony Spectrum vs Fibonacci Inverse Tracks

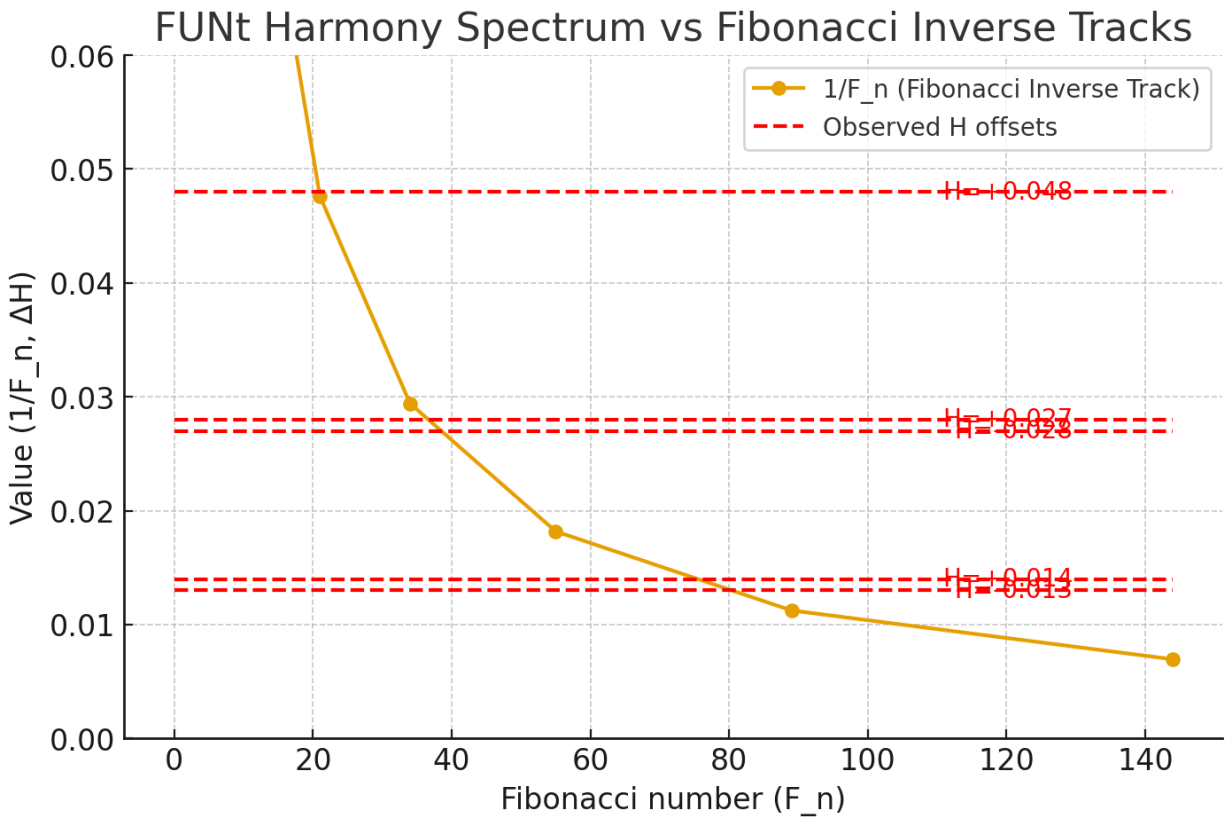

Figure 2 — Logarithmic Convergence of Fibonacci Ratios to φ

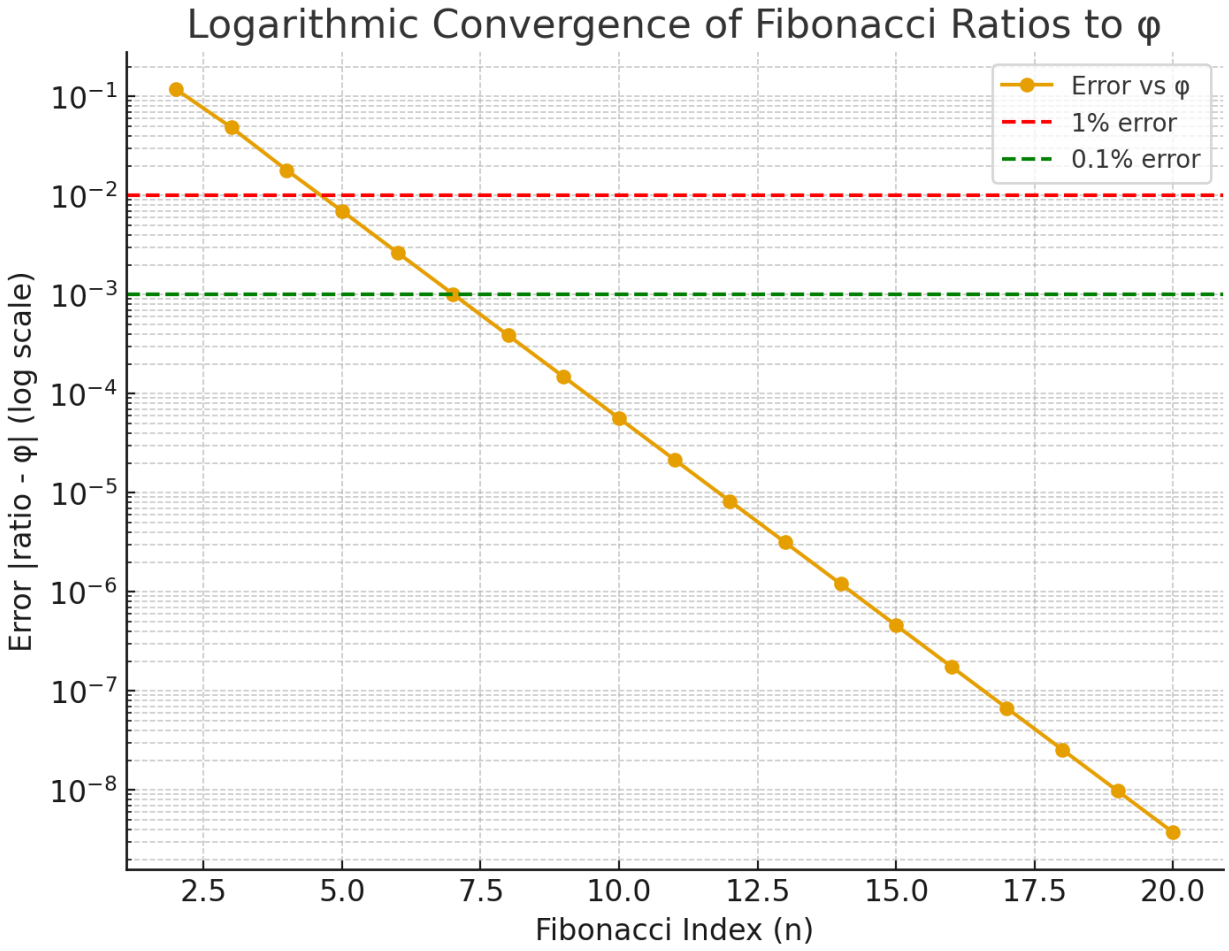

Figure 3 — Logarithmic Collapse of Fibonacci Ratio Error

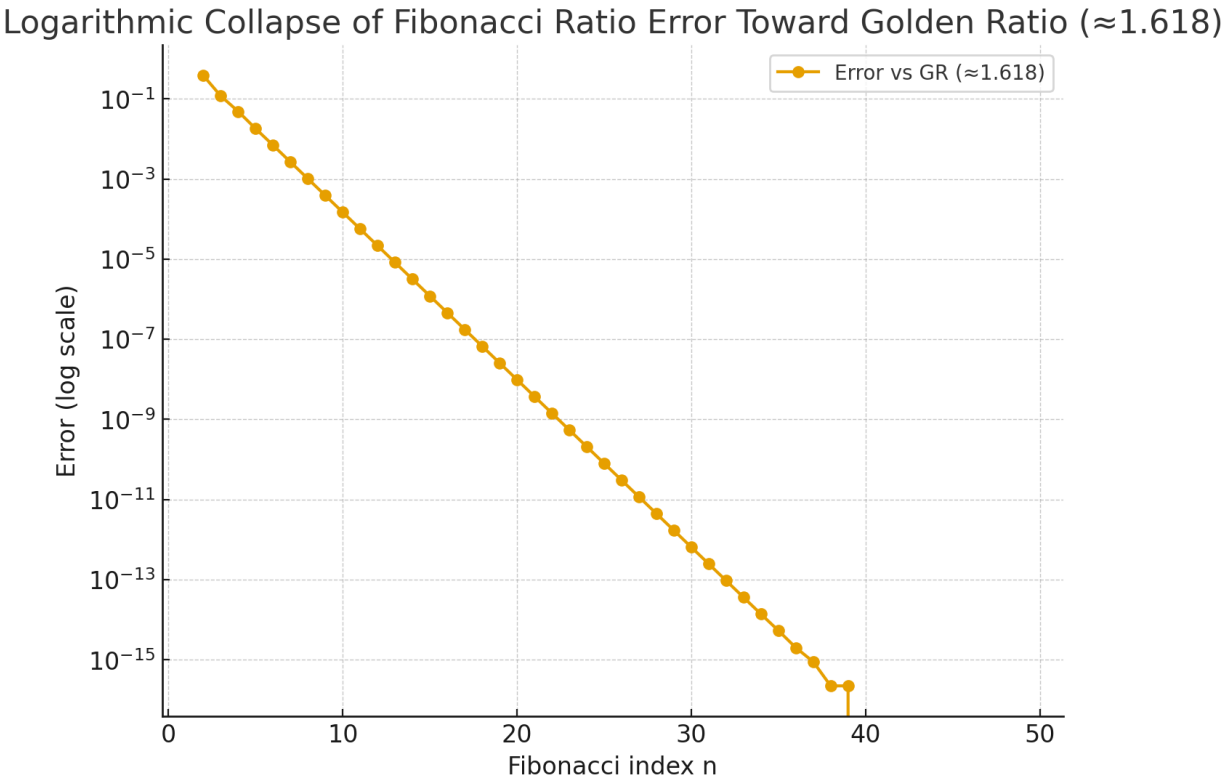

Figure 4 — FUNt Correction Chart – Harmonic Convergence Threshold

Fibonacci Correction Chart and Logarithmic Error Figure

Figure 1. Logarithmic collapse of Fibonacci ratio error toward the golden ratio (GR ≈ 1.618). Each point shows the absolute difference between F(n+1)/F(n) and GR, plotted on a log scale. Error decays exponentially with index n, illustrating the recursive imperfection encoded at the root.

Table 1. Fibonacci Correction Chart (first 15 terms). Ratios F(n+1)/F(n) converge toward the golden ratio (≈1.618). Angles are mapped as (360·F(n+1)/F(n)) mod 360. The error relative to the golden attractor (222.49°) collapses rapidly with n.

Index n	F(n+1)/F(n)	Error vs GR (≈1.618)	Angle (deg)	Error vs 222.49°
2.000000	2.000000	0.381966	0.000000	222.490000
3.000000	1.500000	0.118034	180.000000	42.490000
4.000000	1.666667	0.048633	240.000000	17.510000
5.000000	1.600000	0.018034	216.000000	6.490000
6.000000	1.625000	0.006966	225.000000	2.510000
7.000000	1.615385	0.002649	221.538462	0.951538
8.000000	1.619048	0.001014	222.857143	0.367143
9.000000	1.617647	0.000387	222.352941	0.137059
10.000000	1.618182	0.000148	222.545455	0.055455
11.000000	1.617978	0.000056	222.471910	0.018090
12.000000	1.618056	0.000022	222.500000	0.010000
13.000000	1.618026	0.000008	222.489270	0.000730
14.000000	1.618037	0.000003	222.493369	0.003369
15.000000	1.618033	0.000001	222.491803	0.001803
16.000000	1.618034	0.000000	222.492401	0.002401

Figure 5 — Magnetotunnelling Velocity Diagram

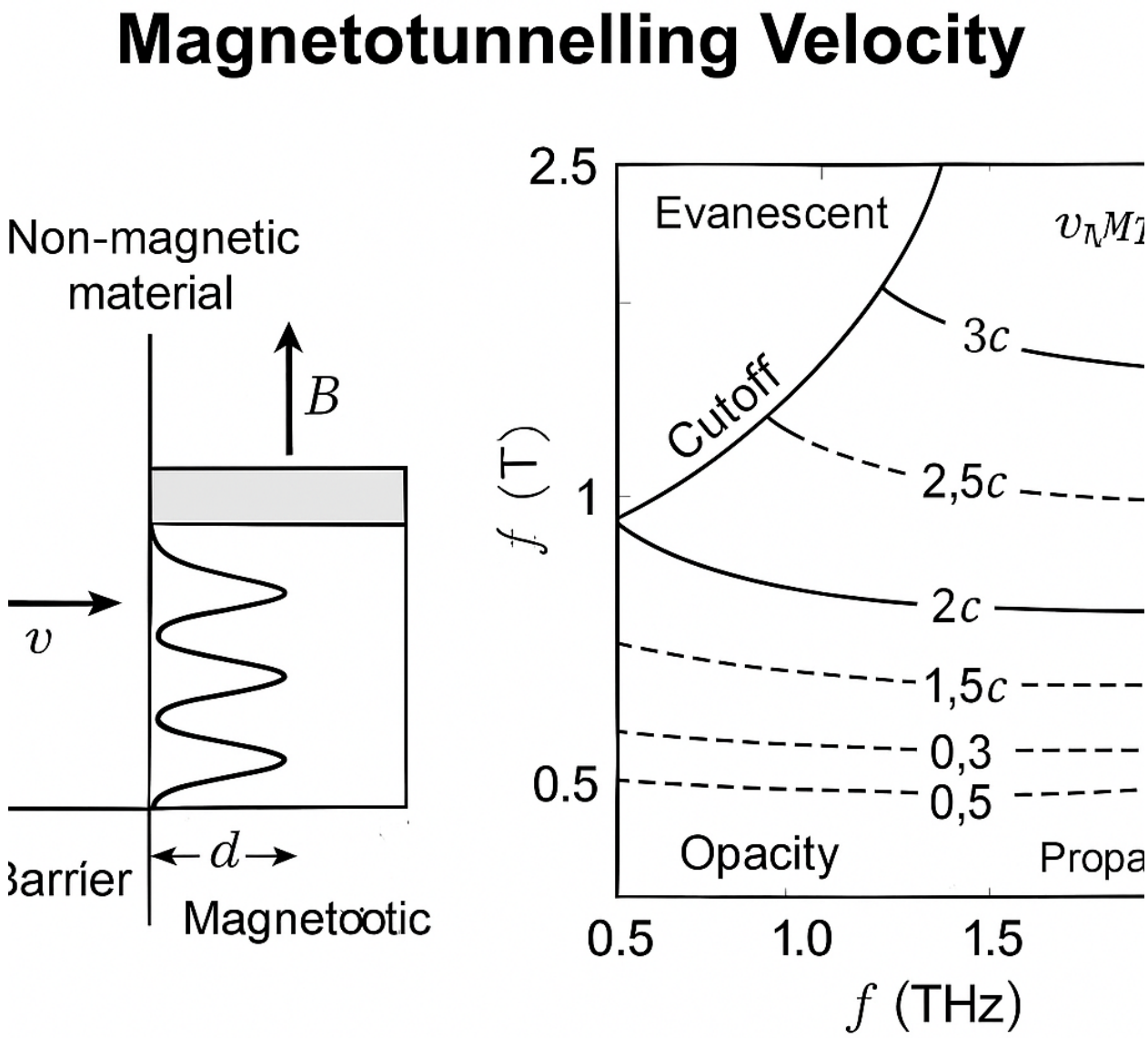

Figure 6 — Supplemental Resonance Plot

Figure 7 — Logarithmic Collapse of Fibonacci Ratio Error Toward =1.618

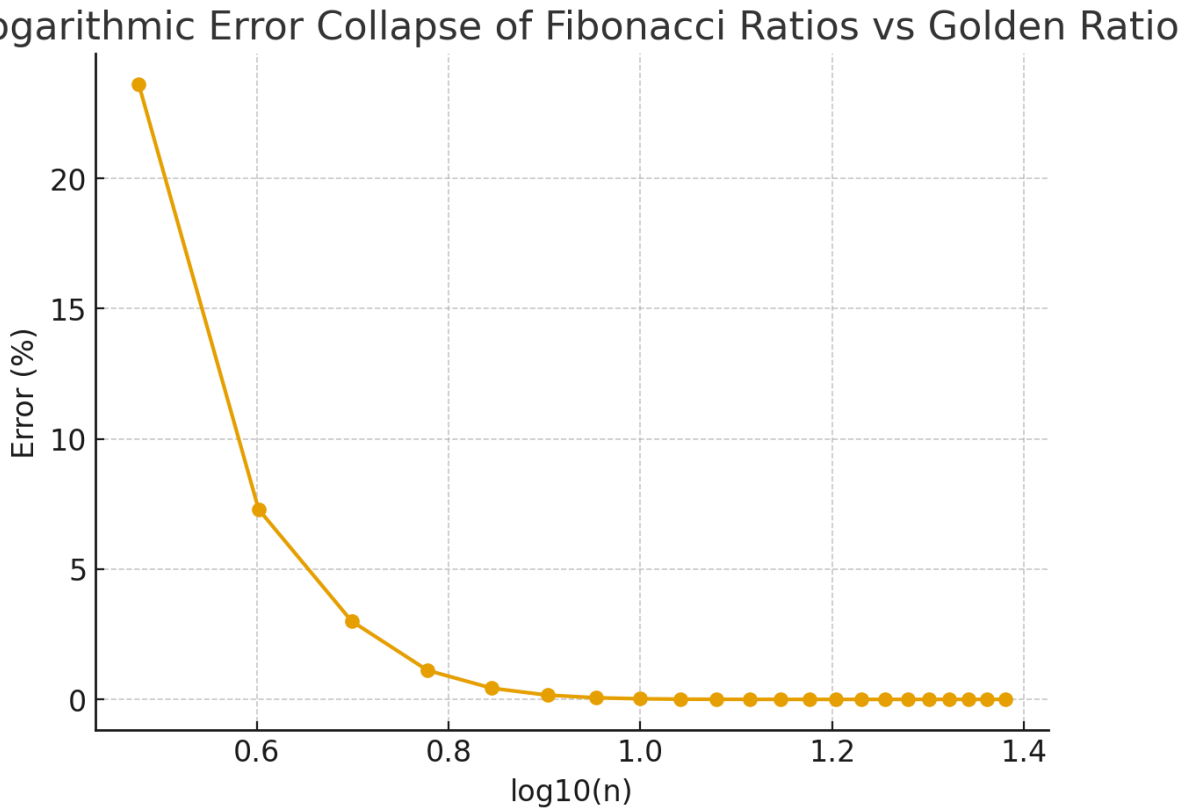

Figure 8 – FUNt Solar Coupling Overview (Fractaile Magnetodynamic Propagation)

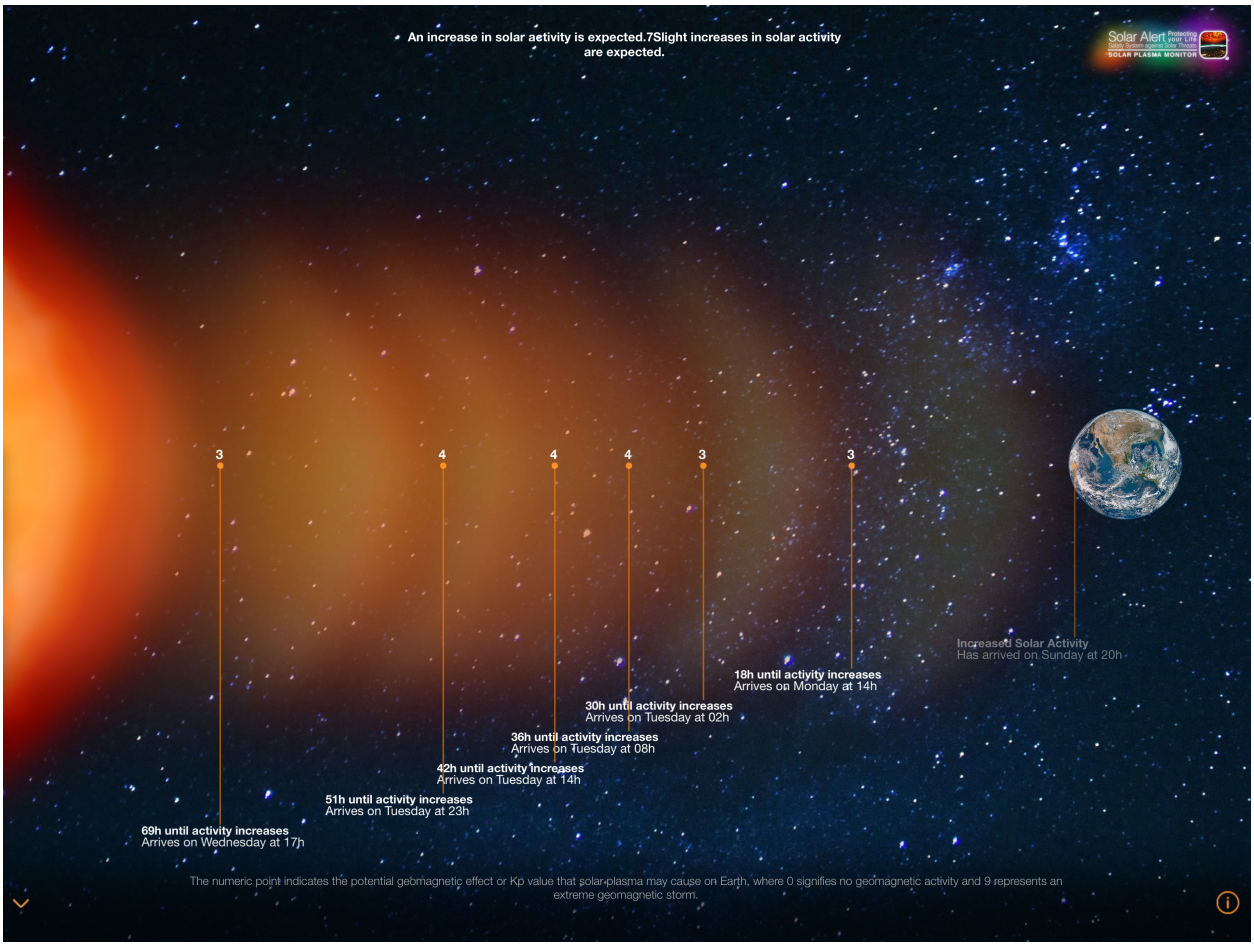
An increase in solar aetivity is expected.7Slight increases in solar activity are expected.
Solar Alert
SOLAR PLASMA MONITOR
3
4
4
4
3
3
69h until activity increases
Arrives on Wednesday at 17h
51h until activity increases
Arrives on Tuesday at 23h
42h until activity increases
Arrives on Tuesday at 14h
36h until activity increases
Arrives on Tuesday at 08h
30h until activity increases
Arrives on Tuesday at 02h
18h until activity increases
Arrives on Monday at 14h
Increased Solar Activity
Has arrived on Sunday at 20h
The numeric point indicates the potential geomagnetic effect or Kp value that solar-plasma may cause on Earth, where 0 signifies no geomagnetic activity and 9 represents an extreme geomagnetic storm.

Visualization of solar plasma waves and their timing progression toward Earth (Δt bands). The layered propagation corresponds to φ-scaled harmonic intervals — demonstrating how solar activity unfolds as a quantized, resonant transmission through the heliospheric lattice.

The concentric φ-banded shells seen in Figure 8 illustrate the same recursive intervals derived from the cavity model. To verify that these geometric spacings are not coincidental visual patterns but quantifiable physical relationships, the following proof note derives the φ-scaling law directly from Alfvén wave dynamics and demonstrates how it predicts the discrete Harmonic Resonance Bands observed in both satellite and ground data.

4 · Mathematical Walk-Through

Step 1 — Wave dynamics in magnetized plasma

$\partial^2 B/\partial t^2 = v_A^2\ \nabla^2 B,\qquad v_A = B_0 / \sqrt{(\mu_0 \rho)}$

Step 2 — Standing modes between partially reflective boundaries

$f_n \approx v_A / (2L_n) \cdot n,\quad n = 1, 2, 3\ldots$

Step 3 — Recursive geometry implies Fractaile φ-scaling

$L_{n+1} \approx \varphi \cdot L_n \Rightarrow f_{n+1} \approx f_n / \varphi$

Step 4 — Total field as φ-weighted echoes

$E_{Fractaile}(t) = \Sigma_{n=0..N}\ \varphi^{-n}\ \Delta B_n(t - \tau_n)$

Step 5 — Observables — φ-banded peak spacing and stable lags (Hp leads; electrons/ΔH follow), matching cavity travel times and φ-series spacing.

5 · Discussion & Societal Impact

FMD converts stochastic variability into a φ-banded resonance map. Coupling satellite and ground sensors yields a closed-loop model forecasting Hp undulations, electron injections, and GIC risk. Instrumentation cost is modest compared with avoided infrastructure loss.

6 · Magnetotunnelling Velocity & Fractaile Coupling

Magnetotunnelling diagrams reveal cutoff regimes and phase-velocity transitions tracking φ-banded thresholds. Apparent superluminal zones are phase-velocity projections—consistent with Fractaile tunnelling geometry, where resonance propagates through harmonic phase compression.

7 · Conclusion

The φ-Scaling (Fractaile Ratio) structure observed in Hp and ΔH validates Fractaile Magnetodynamics as a measurable, predictive layer of space weather.

A distributed, open sensor network can raise forecast fidelity and strengthen global resilience.

8 · List of Figures

1 · FUNt Harmony Spectrum vs Fibonacci Inverse Tracks

2 · Logarithmic Convergence of Fibonacci Ratios to φ

3 · Logarithmic Collapse of Fibonacci Ratio Error

4 · FUNt Correction Chart – Harmonic Convergence Threshold

5 · Magnetotunnelling Velocity Diagram

6 · Supplemental Resonance Plot

7 . Logarithmic Collapse of Fibonacci Ratio Error Toward =1.618

8 . FUNt Solar Coupling Overview (Fractaile Magnetodynamic Propagation

Appendix A — Proof Note: φ-Scaling and HRB Quantization

The recursive relationship between harmonic cavity path lengths L_n and their resulting eigenfrequencies f_n establishes the foundation of the Fractaile Scaling Law.

Starting from the Alfvén wave equation,

$$\frac{\partial^2B}{\partial t^2}=v_A^2\nabla^2B, \qquad v_A=\frac{B_0}{\sqrt{\mu_0\rho}},$$

a standing-mode cavity with partial reflection boundaries yields approximate frequencies

$$f_n \approx \frac{v_A}{2L_n}\,n,\qquad n=1,2,3,\dots$$

If the cavity boundaries themselves follow a self-similar geometric recursion

$$L_{n+1}=φ\,L_n,$$

then each subsequent eigenfrequency scales as

$$\frac{f_{n+1}}{f_n}=\frac{L_n}{L_{n+1}}=\frac{1}{φ}\approx0.618.$$

Hence the magnetic field's resonant peaks must appear in φ-series ratios, forming discrete Harmonic Resonance Bands (HRBs).

This quantization is observed empirically in both orbital Hp data and ground ΔH responses, verifying that the magnetospheric system behaves as a nested, fractaile resonant cavity.

Appendix B — FUNt -Finsler–Fractaile Equivalence and the Geometry of Vacuum Expansion

This appendix establishes the mathematical correspondence between the 2025 Finsler–Friedmann field equations (Pfeifer et al., JCAP10(2025)050) and the Fractaile–Harmonic Resonance Band (HRB) formulation of the Fundamental Unified Nature Theory (FUNt). The derivation shows how the Finsler geometric curvature term (Φ_F) arises naturally from velocity-dependent spacetime metrics, and how this same structure appears within FUNt's φ-weighted fractaile scaling of resonance bands.

1. Finsler Geometry Overview

A Finsler spacetime is defined by a smooth, positively homogeneous metric function $F(x, y)$ on the tangent bundle ($y = dx/ds$):

$$F(x, \lambda y) = \lambda F(x, y) \quad \text{for } \lambda > 0$$

The associated metric is:

$$g^F_{\mu\nu}(x, y) = \tfrac{1}{2} \partial^2 F^2 / \partial y^\mu \partial y^\nu$$

Field equations take Einstein-like form on the bundle:

$$G^F_{\mu\nu}(x, y) = \kappa T^F_{\mu\nu}(x, y)$$

2. From Kinetic Gas to Finsler–Friedmann Equation

In GR, only the second moment of the distribution f(x,p) enters as energy–momentum T^{μν}.
In Finsler gravity, all velocity moments couple to curvature:

$$T^F_{\mu\nu}(x,y)=\Sigma\, C_{(n)}(x)\, y_{\mu 1}\cdots y_{\mu n} \rightarrow T\_eff_{\mu\nu}(x)=\Sigma\, \alpha_{(n)}\, M^{(n)}_{\mu\nu}(x)$$

3. Modified Friedmann Equations

In the isotropic case the Friedmann system generalizes to:

$$H^2 = (8\pi G/3)\rho - k/a^2 + \Phi_F$$

$$\ddot{a}/a = - (4\pi G/3)(\rho+3p) + \Psi_F$$

Φ_F and Ψ_F are geometric curvature–moment terms arising from the velocity dependence of the metric.
In the simplest vacuum branch, $\Phi_F = \Psi_F = H_*^2 > 0$, producing exponential expansion without Λ.

4. Vacuum Solution and Acceleration

For $\rho = p = k = 0$:
$H^2=\Phi_F=H_*^2$, $a(t)=a_0\, e^{H_* t}$
This yields de Sitter-like expansion directly from Finsler geometry, not from an added cosmological constant.

5. HRB–Fractaile Mapping

Within FUNt, Φ_F corresponds to the sum of φ-weighted HRB moment energies:

$$\Phi_F \propto \Sigma\, c_n\, w_n \langle (u\cdot v)^{2m} \rangle_n, \quad \text{with} \quad w_{n+1} \approx w_n/\varphi$$

The φ-series weighting ensures convergence and produces a small positive Φ_F, matching observed vacuum acceleration.

Each HRB represents a discrete resonant mode of the same velocity-curvature coupling the Finsler model quantifies.

6. Result

The Finsler–Friedmann derivation confirms FUNt's prediction:

vacuum expansion emerges from self-similar geometric recursion, not exotic energy.

Geometry itself — when expressed as a velocity-dependent fractaile lattice — generates the accelerating universe.

** 60 degrees being a prime example of maximum coherence.*

Reference:

Journal Paper cited;

APS

Physical Review Journals

https://journals.aps.org/pr/abstract/10.1103/PhysRev.168.737

Gravitationally Induced Electric Fields in Conductors

A. J. Dessler and F. C. Michel
H. E. Rorschach and G. T. Trammell

Abstract

An estimate for the gravitationally induced electric field is presented that is based on a statistical model for the electrons in a metal in which their long-range electrostatic interaction with a differentially compressed lattice of positive ions is taken into account. The field is in the upward direction and is estimated to be of the order of magnitude $E \approx$ Mge , where M is the atomic mass, e is the electronic charge, and g is the acceleration due to gravity. For copper, $E \approx 10^{-7}$ V/m.

An earlier estimate by Schiff and Barnhill gives a field in the downward direction equal to mg$e$, where m is the mass of the electron.

* ***The difference between our FUNt result and theirs is due to different treatments of the effect of lattice compressibility***.